Electronically-Coupled Redox Centers in Trimetallic Cobalt Complexes

Jeremy A. Intrator, Nicholas M. Orchanian, Andrew J. Clough, Ralf Haiges, and Smaranda C. Marinescu*

Department of Chemistry, University of Southern California, Los Angeles, CA, 900089, USA

E-mail: smarines@usc.edu

Keywords: Metal-Organic Frameworks, Electronically-coupled redox centers, Mixed-valent states, Multi-metallic, Electrochemistry

Abstract:

Synthesis and isolation of molecular building blocks of metal-organic frameworks (MOFs) can provide unique opportunities for characterization that would otherwise be inaccessible due to the heterogeneous nature of MOFs. Herein, we report a series of trinuclear cobalt complexes incorporating dithiolene ligands, triphenylene-2,3,6,7,10,11-hexathiolate (THT) (1³⁺), and benzene hexathiolate (BHT) (2³⁺), with 1,1,1,-tris(diphenylphosphinomethyl) ethane (triphos) employed as the capping ligand. Single crystal X-ray analyses of 1³⁺ and 2³⁺ display three five-coordinate cobalt centers bound to the triphos and dithiolene ligands in a distorted square pyramidal geometry. Cyclic voltammetry studies of 1^{3+} and 2^{3+} reveal three redox features associated with the formation of mixed valence states due to the sequential reduction of the redox-active metal centers (Co^{III/II}). Using this electrochemical data, the comproportionality values were determined for 1 and 2 (Log $K_c = 1.4$ and 1.5 for 1, and 4.7 and 5.8 for 2), suggesting strong resonance-stabilized coupling of the metal centers, with stronger electronic coupling observed for complex 2 compared to that for complex 1. Cyclic voltammetry studies were also performed in solvents of varying polarity, whereupon the difference in the standard potentials ($\Delta E_{1/2}$) for 1 and 2 was found to shift as a function of the polarity of the solvent, indicating a negative correlation between the dielectric constant of the electrochemical medium and the stability of the mixed valence species. Spectroelectrochemical studies of in-situ generated multi-valent (MV) states of complexes 1 and 2 display characteristic NIR intervalence charge transfer (IVCT) bands, and analysis of the IVCT transitions for complex 2 suggest a weakly coupled Class II multi-valent species and relatively large electronic coupling factors (1700 cm⁻¹ for the first multi-valent state of 2²⁺, and 1400 and 4000 cm⁻¹ for the second multi-valent state of 2⁺). Density functional theory (DFT) calculations indicate a significant deviation in relative energies of the frontier orbitals of complexes 1^{3+} , 2^{3+} , and 3⁺ that contrasts those calculated for the analogous trinuclear cobalt dithiolene complexes employing pentamethylcyclopentadienyl (Cp*) as the capping ligand (Co₃Cp*₃THT¹ and Co₃Cp*₃BHT², respectively), and may be a result of the cationic nature of complexes 1³⁺, 2³⁺, and **3**⁺.

Introduction

Metal-organic frameworks (MOFs) represent a class of crystalline coordination polymers that display high porosities and surface areas, while also providing access to sorption and catalytic characteristics not displayed in the traditional organic-based polymers.^{3,4} Two-dimensional metalorganic frameworks (2-D MOFs) are a class of MOFs that display structures analogous to that of graphene, with two-dimensional polymeric sheets.^{5,6} Recent studies into this class of modified 2-D conjugated coordination polymers have reported high charge mobilities, conductivities, and porosities. ^{5,6} Importantly, various physical characteristics such as porosity, band gap, conductivity, and magnetic ordering are highly tailorable by altering the metal center, organic ligand, or specific synthetic conditions. This tunability allows for the development of materials with applications in electronics as transistors⁷, capacitors⁸, spintronic devices⁹, and electrocatalysts¹⁰. Conductive 2-D materials have displayed notable activity towards the hydrogen evolution reaction (HER), while also demonstrating band-like metallic conductivity and superconductivity. 8,9,11-24 Due to the heterogeneous nature of MOFs, the fundamental characterization of the metal centers and conjugated organic ligand is a limiting factor for controlling the properties of these materials. As a result, isolating analogous molecular units of MOFs for studies in solution may elucidate physical characteristics that are not directly observable using heterogeneous characterization techniques.

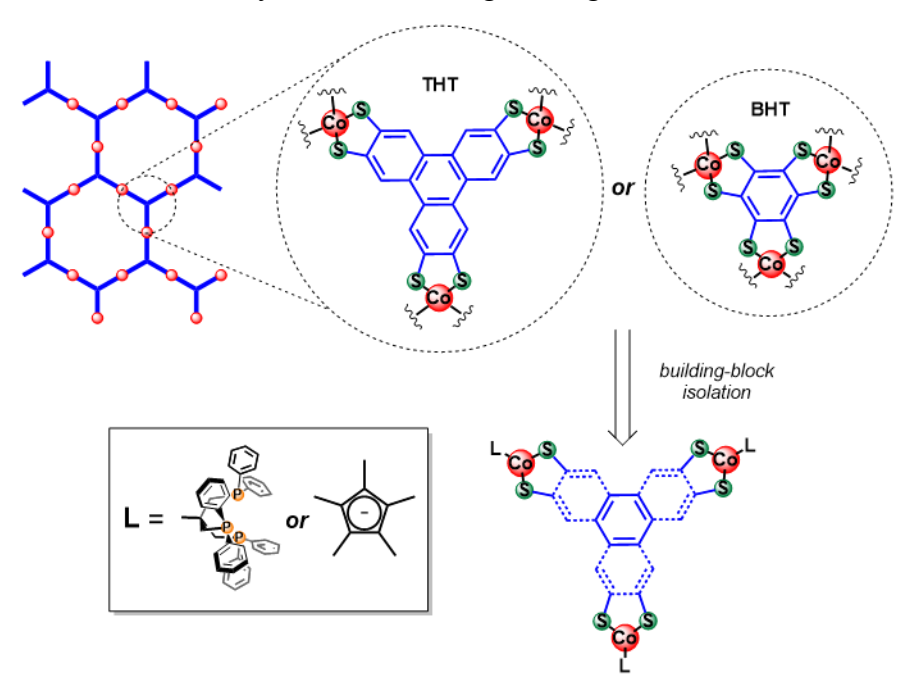


Figure 1. Chemdraw illustrations of the dithiolene-based 2D MOFs containing trinucleating ligands, such as triphenylene-2,3,6,7,10,11-hexathiolate (THT) and benzene hexathiolate (BHT), and the proposed homogenization strategy of the cobalt-dithiolene molecular units.

The isolation of molecular building blocks of 2-D MOFs for study can be achieved by the addition of capping ligands, which hinder polymerization, resulting in the formation of multimetallic complexes (Figure 1). Due to the highly coupled nature of the redox-active moieties, many studies have been conducted on this class of multimetallic complexes employing various

ligand architectures, metals, and capping ligands to investigate the electronic properties of these complexes. A trimetallic complex incorporating a trinucleating hexahydroxytriphenylene (HHTP) ligand coordinating three ruthenium bis(bipyridine) centers was reported to display strong coupling between the redox-active dioxolene ligands, resulting in stabilization of intermediate redox states. 25 Analogous copper and nickel-coordinated HHTP complexes were also investigated and shown to display similar electronic coupling between the redox-active sites, suggesting that this electronic communication mechanism occurs in the associated 2-D MOF material as well. 26,27 Attempts to study the copper-coordinated hexaiminotriphenylene congener through electrochemical studies were hindered by the instability of this complex to disproportionation under reductive conditions.²⁶ Lastly, tri-nucleating complexes employing the dithiolene-based triphenylene-2,3,6,7,10,11-hexathiolate (THT)¹ and benzene hexathiolate (BHT)² ligands (Co₃Cp*₃THT and Co₃Cp*₃BHT, respectively, for the cobalt-based derivatives) with pentamethylcyclopentadienyl (Cp*) as the capping ligand, have previously been reported incorporating group 9 and 10 metals. These complexes notably exhibit metal-based redox-active centers and display strong electronic communication between the metal centers, evidenced by electrochemical and spectroscopic studies, with metallic coupling strongly affected by the choice of dithiolene bridging ligand and the metal center.

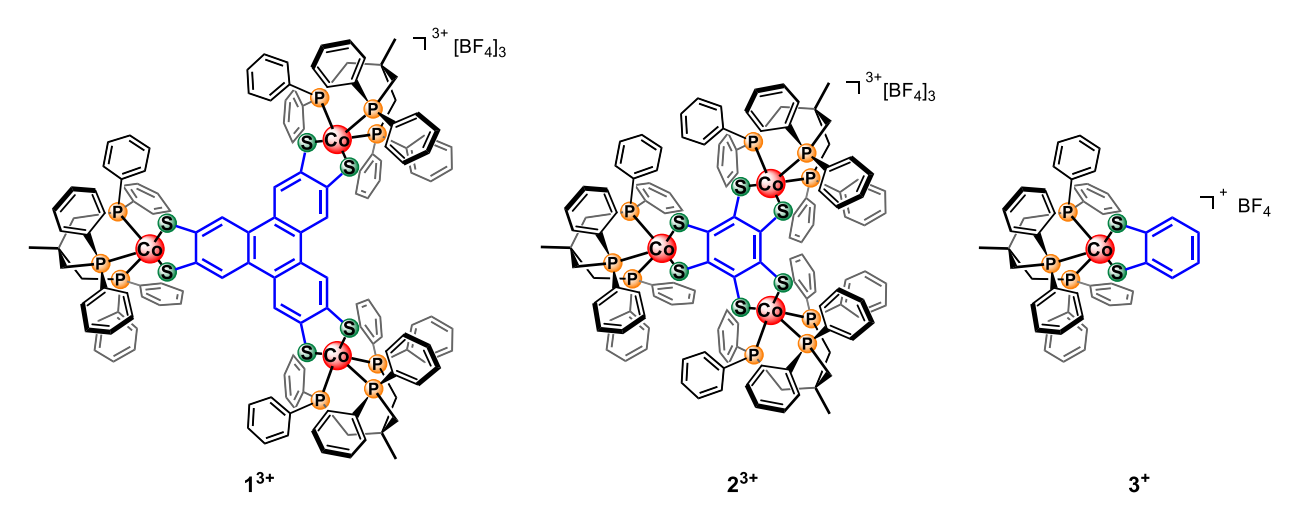


Figure 2. Chemdraw illustration of the synthesized trimetallic complexes 1^{3+} and 2^{3+} , and the monometallic analogue 3^+ studied here.

Herein, we report two new trinuclear cobalt complexes incorporating dithiolene ligands, such as triphenylene-2,3,6,7,10,11-hexathiolate (THT) (1³⁺), and benzene hexathiolate (BHT) (2³⁺), with 1,1,1,-tris(diphenylphosphinomethyl) ethane (triphos) employed as the capping ligand (Figure 2). Inspired by the results from similar THT¹ and BHT² complexes mentioned above, as well as our previous studies detailing BHT- and THT-based 2-D MOFs^{17–21,28}, we have investigated the influence of the coordination environment and the electrochemical medium on the electronic coupling between the metal centers. Consequently, the complexes described herein can serve as molecular models to provide complementary insight into the electronic properties of the materials with THT and BHT ligands. X-ray crystallography, UV-Vis-NIR spectroscopy, and electrochemical studies were carried out to investigate the electronic coupling of the redox active

metal centers in complexes 1 and 2, and these results are supported through density-functional theory (DFT) calculations. We further compare these results to previously-reported Co₃Cp*₃THT¹ and Co₃Cp*₃BHT² systems to highlight the influence of the capping ligand on the electronic structure of these model complexes. A mononuclear cobalt complex [Co(triphos)(BDT)][BF4] (3+), where BDT = 1,2-benzenedithiolate, was synthesized and studied to highlight the electronic effects resulting from the multimetallic nature of complexes 1 and 2 (Figure 2), and to probe the effect of capping ligand relative to the Cp*- analogue (CoCp*BDT).¹

Results and Discussion

Scheme 1. Synthetic procedure for complexes 1^{3+} and 2^{3+} .

Complex 1³⁺ was synthesized via a two-step one-pot process (Scheme 1). First, 1,1,1tris(diphenylphosphinomethyl)ethane (triphos) was added to cobalt(II) tetrafluoroborate in acetonitrile literature procedure²⁹ following published form cobalt(triphos)(tetrafluoroborate) complex. Subsequent addition of the THT ligand to the reaction mixture in the presence of triethylamine led to the formation of a red precipitate. After overnight stirring, the mixture was exposed to ambient atmospheric conditions, whereupon any apparent red precipitate dissolved to generate a blue solution. After removal of the volatiles and washing with THF, complex 1³⁺ was isolated as a blue powder. The ¹H nuclear magnetic resonance (NMR) spectrum of 1^{3+} in DMSO- d_6 displays sharp features, indicative of a diamagnetic species (Figure S1). Two broad aliphatic singlets are observed at δ 2.98 and 2.00 ppm in a 6:3 ratio, corresponding to the methylene and methyl moieties on the triphos ligand, respectively. Four aromatic signals

appear at δ 9.93 (s), 7.29 (t), 7.18 (m), and 7.10 (t) ppm in a 2:6:12:12 ratio, corresponding to the protons of the triphenylene core (δ 9.93 ppm), and the aryl substituents of the triphos ligand (δ 7.29-7.10 ppm range). The ¹⁹F-{¹H} NMR spectrum of **1**³⁺ in DMSO- d_6 displays one fluorine environment at δ -148.0 ppm, corresponding to the BF₄⁻ anion (Figure S3). The presence of the BF₄⁻ counteranion, along with the observation of a diamagnetic species by ¹H NMR spectroscopy, suggests that complex **1**³⁺ contains Co(III) centers. The ³¹P-{¹H} NMR spectrum of **1**³⁺ displays a single broad peak at δ 33.8 ppm, corresponding to the triphos ligand (Figure S2).

The synthetic procedure for complex 2^{3+} was similar to that of complex 1^{3+} . BHT was added to the in situ generated cobalt(II)(triphos)(tetrafluoroborate) complex in the presence of triethylamine to directly form a green-blue solution. After overnight stirring, the mixture was exposed to ambient atmospheric conditions, where the solution color changed from green to blue. After removal of the volatiles and subsequent washings, complex 2³⁺ was isolated as a blue powder. The ¹H NMR spectrum of 2³⁺ in DMSO-d₆ also displays sharp features, indicative of a diamagnetic species (Figure S4). Two broad aliphatic singlets are observed at δ 2.97 and 2.01 ppm in a 6:3 ratio, assigned to the triphos methylene (CH_2) and methyl (CH_3) moieties, respectively. Three aromatic signals appear at δ 7.20 (t), 7.15 (m), and 6.88 (t) ppm, in a 6:12:12 ratio, representing the protons of the aryl substituents of the triphos ligand. The ¹⁹F-{¹H} NMR spectrum of 2^{3+} in DMSO- d_6 displays one fluorine environment at δ -148.0 ppm, corresponding to the BF₄⁻ anion (Figure S6). Similar to complex 1³⁺, the presence of the BF₄ counteranion, along with the observation of a diamagnetic species by ¹H NMR spectroscopy, suggests that complex **2**³⁺ contains Co(III) centers. The ${}^{31}P-{}^{1}H$ NMR spectrum of 2^{3+} displays one broad peak at δ 31.4 ppm, corresponding to the triphos ligand (Figure S5). Synthesis of complex 3⁺ was adapted from the literature³⁰, incorporating tetrafluoroborate as the counter-anion instead of the reported hexafluorophosphate to allow for accurate comparisons of the complexes synthesized (Figures S7-S9). The ¹⁹F-{¹H} NMR spectrum of 3^+ in DMSO- d_6 displays one fluorine environment at δ -148.0 ppm, indicating the successful incorporation of the BF₄ anion (Figure S9).

X-ray photoelectron spectroscopy (XPS) surveys on crystals of complexes 1³⁺, 2³⁺, and 3⁺ confirm the presence of Co, S, P, C, F, and B (Figures S10-S15). The high-resolution scans of the Co 2p region for complexes 1³⁺ and 2³⁺ display similar features at binding energies of 794.7 eV and 779.8 eV for complex 1³⁺ and 794.9 eV and 779.9 eV for complex 2³⁺, corresponding to the Co 2p_{1/2} and 2p_{3/2} levels, respectively. Analogous scans of the Co 2p region for complex 3⁺ display features at binding energies of 795.2 eV and 780.2 eV, indicating a small shift in the 2p_{1/2} and 2p_{3/2} levels toward higher binding energies. The Co 2p regions for complexes 1³⁺, 2³⁺, and 3⁺ display no satellite features at 786 eV, suggesting that the cobalt centers for each complex are in the formal +3 oxidation states (i.e. Co^{III}). High resolution scans of S 2p and P 2p regions of complexes 1³⁺, 2³⁺, and 3⁺ show features at binding energies of 163.9 eV and 162.7 eV, corresponding to the S 2p_{1/2} and S 2p_{3/2} levels, respectively, and 132.4–132.5 eV and 131.5–131.6 eV, corresponding to the P 2p_{1/2} and P 2p_{3/2}, respectively. Lastly, high resolution scans of the F 1s and B 1s regions display characteristic peaks at 685.3–684.9 eV and 193.8 eV, respectively, reflecting the presence of the BF₄⁻ anion.

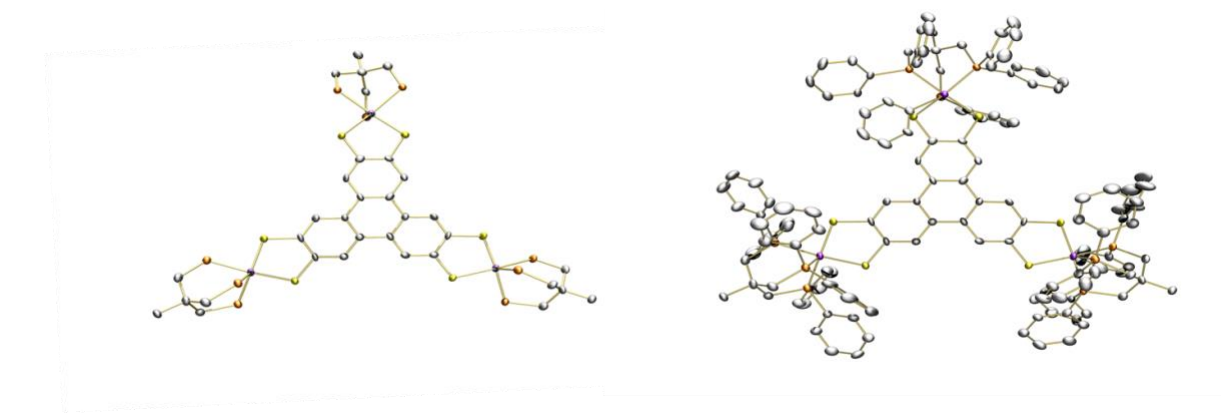


Figure 3. Top-down view of the solid-state structure of complex 1^{3+} . Aryl and aliphatic protons, counterions, and solvent molecules are omitted for clarity.

X-ray quality crystals of complex 1^{3+} were grown via vapor diffusion of diethyl ether into an acetonitrile solution containing complex 1^{3+} , and a solid-state crystal structure was obtained (Figures 3, S16, and S17, and Tables 1, S6, and S7). Notably, to our knowledge, this is the first solid state structure reported for a triphenylene-based Co-dithiolene trimetallic complex. Single crystal X-ray analysis of 1^{3+} indicates a species containing three cobalt metal centers, each coordinated to a central THT ligand and capped with a single triphos ligand. Additionally, BF₄- anions were detected in the lattice as outer-sphere counterions. Three BF₄- counteranions are present for each molecular unit in the lattice, suggesting that complex 1^{3+} has an overall charge of +3 and that each Co center has a +3 formal oxidation state. The angular structural parameter, τ , was calculated to be <0.1 for each metal center (Equation S1), suggesting that each cobalt center adopts a distorted square pyramidal geometry.

Table 1. Average selected bond lengths (Å) for complex 1³⁺.

Bond	Bond
	Length
	(Å)
Co-S	2.159(2)
Co-	2.173(5)
Papical	
Co-	2.241(4)
Pbasal	
C-S	1.736(5)

Average selected bond lengths and angles can be found in Tables 1 and S7. We can identify two asymmetric Co–P bonding environments within the structure; one environment is within the basal plane of the square pyramidal coordination sphere (labeled as Co– P_{basal}), and the other is perpendicular to the square pyramidal plane (labeled as Co– P_{apical}). Comparing the same Co–P bonding environments reported in the solid state structure for complex $\bf 3^+$ (Co– P_{apical} : 2.183(2) Å, Co– P_{basal} : 2.232(2) Å)³¹, we find that complex $\bf 1^{3+}$ displays slightly shorter Co– P_{apical} bond lengths (by ~0.010 Å) and slightly longer Co– P_{basal} bond lengths (by ~0.009 Å). The average Co–S bond

for complex 1³⁺ is measured to be 2.159(2) Å, which is slightly shorter than the Co–S bond reported for complex 3⁺ (2.169 (2) Å)³¹. Complex 1³⁺ exhibits an average bond length of 1.736(5) Å for the C–S bond, which is in good agreement with reported dithiolene ligands in their reduced thiolate state, further supporting the +3 oxidation assignment of the metal centers.³² Significant bowing is apparent in the triphenylene backbone, with an angle of 22.6(7)° between the plane of the central six carbon atoms of the triphenylene core and that of the asymmetric cobalt-dithiolene moiety (Figure S16). This is ascribed to a crystal packing effect, similar to the bowing of internal ligands observed in analogous complexes.¹

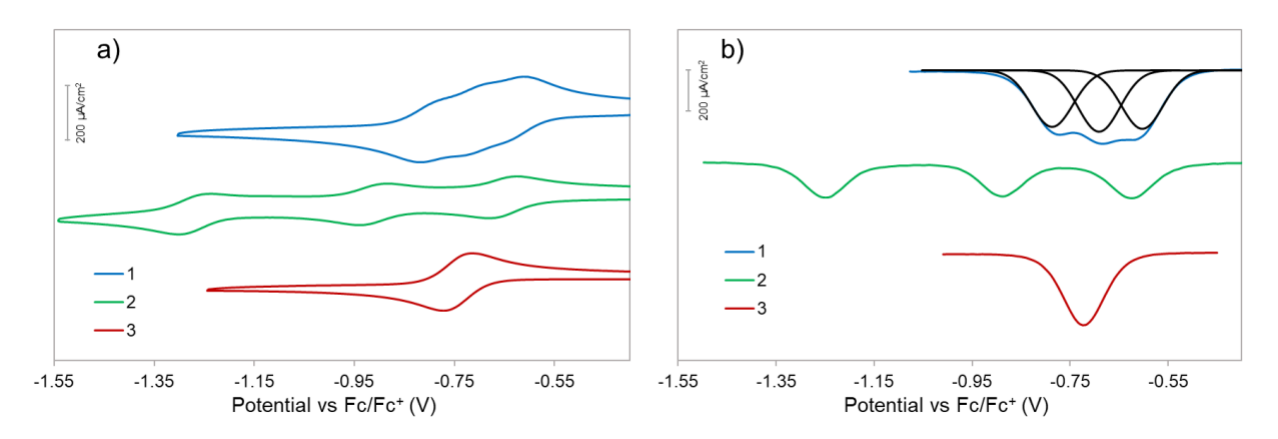


Figure 4. a) CVs of complexes **1–3** (0.5 mM) and b) DPVs of **1–3** (0.5 mM) in MeCN solutions containing 0.1 M [*n*Bu₄N][PF₆] under an atmosphere of N₂. Scan rate is 100 mV/s.

Cyclic voltammetry (CV) studies of complexes 1^{3+} , 2^{3+} , and 3^+ (0.5 mM) under N₂ atmosphere were carried out using a glassy carbon working electrode in acetonitrile (MeCN) solutions with 0.1 M tetrabutylammonium hexafluorophosphate ([nBu_4N][PF₆]) as the supporting electrolyte. All potentials are referenced versus Fc^{+/0} and all CVs were first scanned cathodically and subsequently returned anodically. CV studies of complex 1 display a reversible redox feature centered at -0.69 V, which can be deconvoluted using differential pulse voltammetry (DPV) to separate three reversible one-electron events with standard potentials ($E^0_{1/2}$) at -0.63 V, -0.71 V, and -0.80 V (Figure 4). Analogous metal dithiolene complexes have shown similarly convoluted redox features, assigned to the sequential reduction of electronically-coupled redox-active metal centers. ^{1,33} Similar electrochemical behavior is observed for complex 1, and is therefore attributed to electronic coupling between the cobalt centers in this trimetallic system.

CV studies of complex 2 display three reversible one-electron features with standard potentials ($E^0_{1/2}$) at -0.65 V, -0.93 V, and -1.27 V, with a greater degree of separation relative to those observed in complex 1. These three separate reversible one-electron events can be similarly associated with electronic coupling between the cobalt centers, comparable in nature to what is observed for complex 1. The shift of each sequential $E^0_{1/2}$ for complex 2 can be attributed to the increased stability of the mixed-valent species, due to stronger electronic coupling of the redox active sites through the central benzene ligand compared to the bridging triphenylene ligand of complex 1. CV studies of complex 3 exhibit a single reversible redox feature at -0.74 V, which was previously assigned to the Co^{III/II} couple (Figure 4a). As only one reduction feature was

observed for complex **3** within the potential range studied, the three redox features of **1** and **2** can also be attributed to sequential Co^{III/II} couples for each metal center. Randles-Sevcik plots for complexes **1–3** (Figures S21–S23) in acetonitrile yield slopes of approximately 0.5 (Figures S24–S28), as expected for freely diffusing molecular species in solution.

As the metal centers in complexes 1 and 2 are sequentially reduced, mixed valence (MV) states are formed. A comproportionality constant (K_c) for the formation of the MV state relative to disproportionation can be described using the following equation:

$$K_c = \frac{[X^n]^2}{[X^{n+1}][X^{n-1}]} = \exp\left\{ \left[E_{\frac{1}{2}}^0 (X^{n+1}/X^n) - E_{\frac{1}{2}}^0 (X^n/X^{n-1}) \right] F/RT \right\} = \exp\left\{ \Delta E_{\frac{1}{2}}^0 F/RT \right\} \quad (1)$$

where n is the charge, [Xⁿ] is the concentration of the MV species with charge n, [Xⁿ⁺¹] and [Xⁿ⁻¹] are the concentrations of the isovalent species, and $E^0(X^{n+1}/X^n)$ and $E^0(X^n/X^{n-1})$ are the standard potentials of the respective species. ^{1,34,35} In the case of complexes 1 and 2 there are three separate redox couples consisting of $E^0(X^{2+/3+})$, $E^0(X^{1+/2+})$, and $E^0(X^{+/0})$, generating two possible MV states, X^{2+} for the [Co^{II}Co^{III}Co^{III}] species and X^+ for the [Co^{II}Co^{III}Ol^{III}] species, resulting in two separate $\Delta E_{1/2}$ and K_c values for each state (Figure 5). The Log K_c values of both states of complex 1 and 2, labeled as X^{2+} for $\Delta E_{1/2}[(X^{3+}/X^{2+}) - (X^{2+}/X^{1+})]$ and X^+ for $\Delta E_{1/2}[(X^{2+}/X^+) - (X^+/X^0)]$, are presented in Table 2.

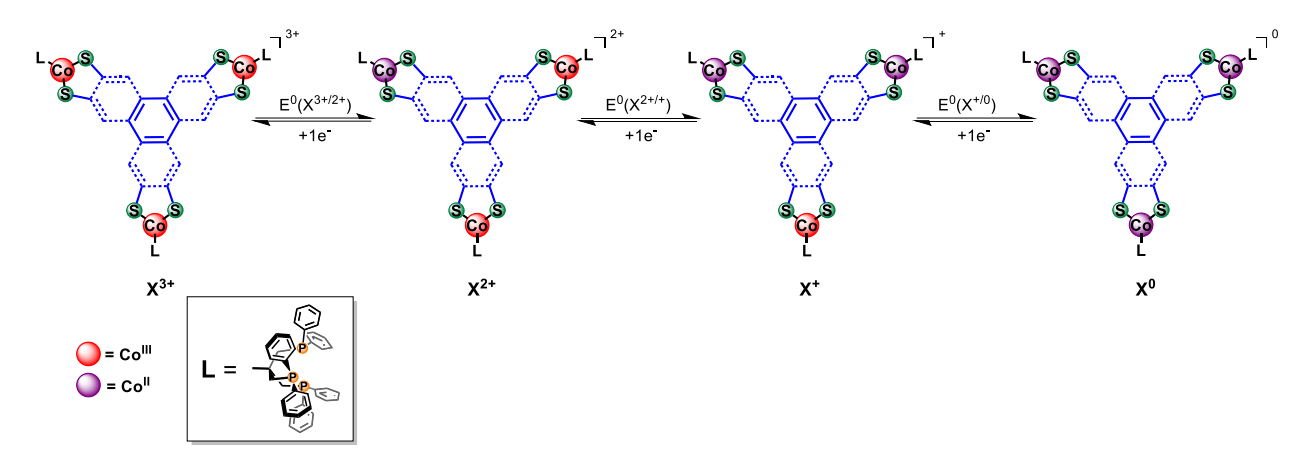


Figure 5. Chemdraw illustrations of multi-valent states of complexes 1 and 2 accessible through electrochemical studies.

Table 2. The comproportionality constants determined based on the Co^{III/II} redox couples present in complexes 1 and 2 (in MeCN) and those reported for Co₃Cp*₃THT and Co₃Cp*₃BHT.

Complex	E^0 1/2	E^0 1/2	E^0 1/2	Log	Log	Ref
	(X^{3+}/X^{2+})	(X^{2+}/X^+)	(X^+/X^0)	$K_c(X^{2+})$	$K_c(X^+)$	
	(V vs	(V vs	(V vs			
	Fc/Fc^{+})	Fc/Fc^{+})	Fc/Fc^{+})			

1	-0.63	-0.71	-0.80	1.4	1.5	This work
2	-0.65	-0.93	-1.27	4.7	5.8	This work
Co ₃ Cp* ₃ THT	-1.31	-1.38	-1.46	1.2	1.4	1
Co ₃ Cp* ₃ BHT	-1.35	-1.58	-1.92	3.9	5.8	2

The free energy of comproportionation of the MV species relies on various thermodynamic factors including contributions from inductive, electrostatic, and magnetic effects in addition to resonance-based stabilization effects.³⁵ While the degree of comproportionation cannot directly indicate the magnitude of the resonance-stabilized coupling in MV species, it can provide a diagnostic handle in comparing relative changes in electronic coupling in structurally similar systems.^{36,37} The K_c values measured for complex 2 is several orders of magnitude larger than that of complex 1 (>10⁴), which is likely a result of the stronger coupling of the metal centers through the bridging benzene ligand of complex 2. The measured K_c values for complexes 1 and 2 are comparable to those reported for Co₃Cp*₃THT and Co₃Cp*₃BHT, since the electronic coupling is primarily through the conjugated THT and BHT ligands, respectively (Table 2). Notably, the sequential Co^{III/II} couples for complexes 1 and 2 are shifted to more positive potentials (by >70 mV) compared to those reported for Co₃Cp*₃THT and Co₃Cp*₃BHT, likely due to the neutral capping triphos ligand in contrast to the anionic Cp* ligand.

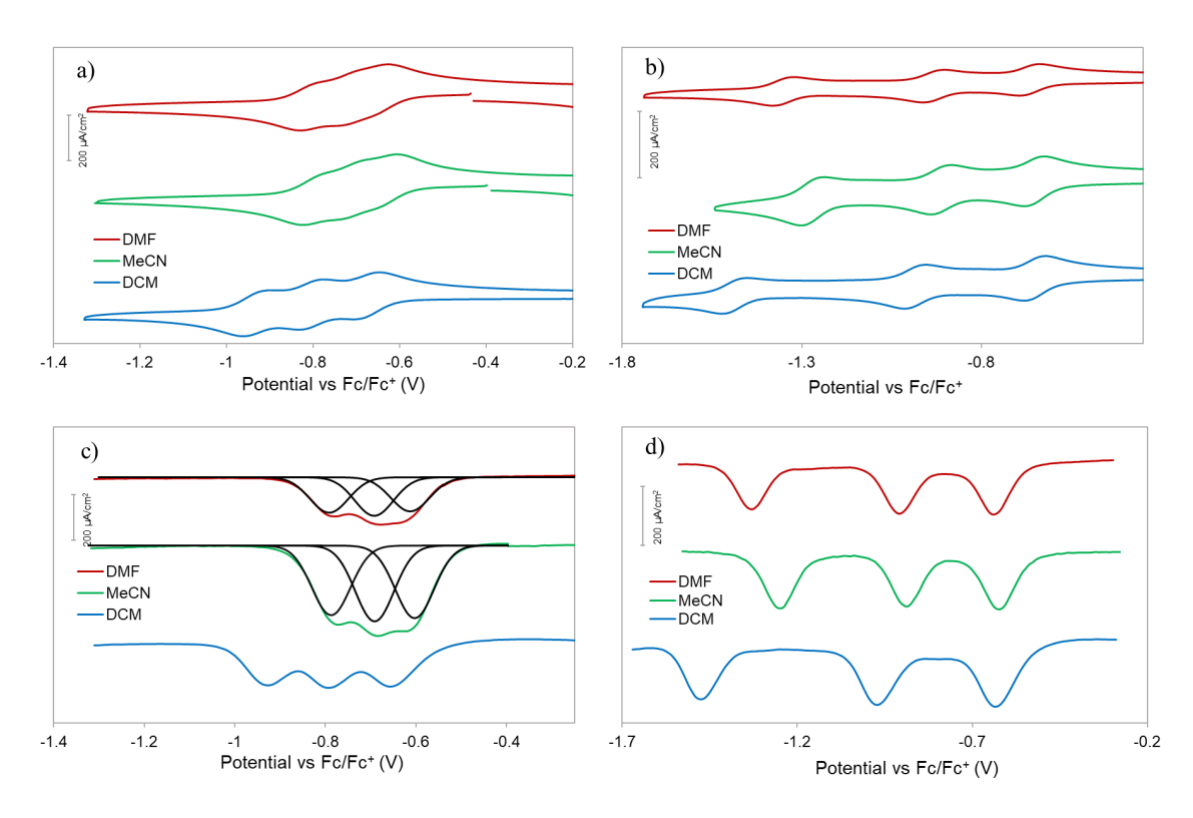


Figure 6. CVs and DPVs of **1** (0.5 mM) (a,c) and **2** (0.5 mM) (b,d) in a solution containing 0.1 M [nBu₄N][PF₆] under an atmosphere of N₂ in DMF (red), MeCN (green), and DCM (blue). Scan rate is 100 mV/s.

Additional factors such as solvation effects can contribute significantly to the stability of mixed valence states, and $\Delta E_{1/2}$ values are expected to shift in conjunction with solvent polarity. CV studies of complexes $\mathbf{1}^{3+}$ and $\mathbf{2}^{3+}$ were performed in dichloromethane (DCM) and N,N-dimethylformamide (DMF) to determine the effect of solvent polarity on stabilization of the mixed-valency of both complexes (Figures 6 and S29–S42). The $\Delta E_{1/2}$ values observed in each solvent for the Co^{III/II} couples of complexes $\mathbf{1}$ and $\mathbf{2}$ can be found in Table 3.

Table 3. Calculated $\Delta E_{1/2}$ of the Co^{III/II} redox couples for complexes **1** and **2** in DMF, MeCN, and DCM, where ΔE refers to the difference in the reduction potential of the first and second redox event ($\Delta E^{\rm a}$) and of the second and third redox event ($\Delta E^{\rm b}$) for the respective species.

Solvent	Dielectric	$\Delta E^a(X^{3+/2+}$	$\Delta E^b(\mathrm{X}^{2+/+}$ -	$\Delta E^a(X^{3+/2+}$	$\Delta E^b(\mathbf{X}^{2+/+}$ -
	Constant ³⁸	$X^{2+/+}$) for 1	$X^{+/0}$) for 1	$X^{2+/+}$) for 2	$X^{+/0}$) for 2
DMF	38.25	80	101	270	420
MeCN	36.65	80	100	260	360
DCM	8.93	139	126	340	500

As the solvent polarity decreases from MeCN to DCM, a marked increase is observed in the $\Delta E_{1/2s}$ for complexes 1 and 2. Previous studies on the behavior of MV systems have

demonstrated that low-polarity, low-donor strength solvents (such as DCM) increase MV stability. 39,40 The capacity of the solvent to electronically shield the charged metal centers on complexes 1 and 2 is directly associated with its dielectric constant. As the metal centers of the isovalent states have a higher intrinsic electrostatic repulsion compared to the MV state (the difference in charge in Equation 1 is always 1, electrostatically favoring the MV state), solvents of high dielectric constants can shift the equilibrium towards the isovalent species relative to the MV species due to greater stabilization of this coulombic repulsive force by dielectric shielding. 41,42 Additionally, solvents with relatively high intrinsic Lewis basicity, such as MeCN, can localize charge on the cationic metal centers via inductive effects, reducing delocalization as a stabilizing feature in MV species. 40,43 Moreover, solvents of low polarity may also favor the solvation of the partially reduced MV states of complexes 1 and 2, as the cationic charge is sequentially reduced, thus favoring the less polar solvents such as DCM.³⁹ It should be noted that utilization of solvents of low polarity have also been reported to increase ion-pairing effect due to a decrease in solvation of both the MV species and electrolyte in solution. This effective increase in ion-analyte interaction has been reported to accentuate the effect of the electrolyte ion identity as the primary means of affecting $\Delta E_{1/2}$ Notably, this trend is not observed in the CV studies of complexes 1 and 2 in the stronger donating solvent DMF. Comparison of the $\Delta E_{1/2}$ values of complexes 1 and 2 in MeCN and DMF demonstrates the opposite trend, where an increase in the $\Delta E_{1/2}$ is observed in the more donating DMF, albeit a weaker shift compared to the one observed upon switching from MeCN to DCM. Randles-Sevcik analysis was performed on complexes 1 and 2 in both DMF and DCM, confirming that the trimetallic complexes are freely-diffusing at the electrode's double-layer in these solvents as well (Figures S29–S42).

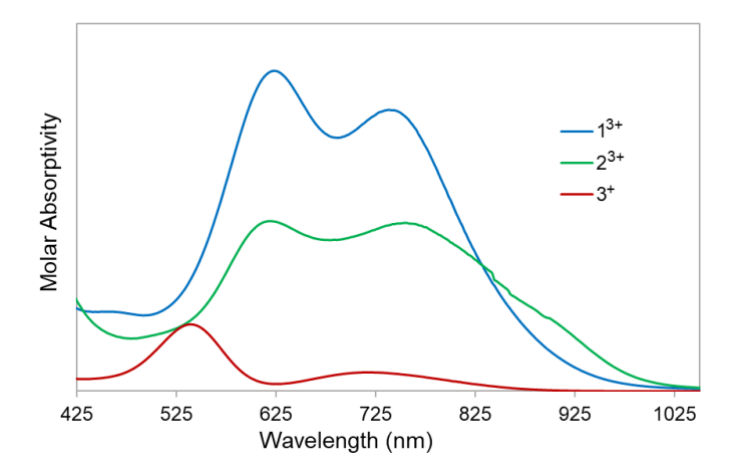


Figure 7. Visible absorbance spectra of complexes 1^{3+} , 2^{3+} , and 3^{+} in acetonitrile.

Table 4. λ_{max} and molar absorptivity values for 1^{3+} , 2^{3+} , and 3^{+} in the visible range.

Complex	Transition	$\lambda_{max}(nm)$	ε (10 ⁻⁴ M ⁻¹ cm ⁻¹)
1 ³⁺	λι	624	3.49(0.04)
	λ_2	738	3.17(0.04)

2 ³⁺	λ_1	618	1.83(0.04)
	λ_2	756	1.88(0.04)
3 ¹⁺	λ_1	540	0.73(0.02)
	λ_2	720	0.204(0.002)

To further probe the electronic structure of these complexes, UV-Vis absorption spectroscopy studies were performed on complexes 1^{3+} , 2^{3+} , and 3^+ in acetonitrile. Absorbance spectra of these species show two peaks in the visible range (Figures 7, S18–S20). The wavelengths of maximum absorption (λ_{max}) and molar absorptivities (ϵ) are displayed in Table 4. Complexes 1^{3+} and 2^{3+} display prominent transitions (λ_1) at 624 nm and 618 nm, respectively, consistent with charge-transfer transitions. Additionally, weaker transitions at longer wavelengths (λ_2) were detected at 738 nm for complex 1^{3+} , and 756 nm for complex 2^{3+} . These absorptions were not observed for $\mathbf{Co_3Cp^*_3THT}$ or $\mathbf{Co_3Cp^*_3BHT}$, suggesting substantial contribution from the triphos capping ligand. A slight blue shift in λ_1 was observed for complex 1^{3+} relative to complex 2^{3+} (by 6 nm), as well as a red shift in λ_2 (by 18 nm). The UV-vis spectrum of complex 3^+ displays a prominent transition at 540 nm (λ_1), and a weaker absorption at 720 nm (λ_2). The absorption peaks for complex 3^+ are blue-shifted compared to those of complex 1^{3+} (by 84 nm for λ_1 and 18 nm for λ_2) and complex 2^{3+} (by 78 nm for λ_1 and 36 nm for λ_2).

To further investigate the degree of electronic coupling in complexes 1 and 2, MV states of complexes 1 and 2 were electrochemically generated and studied using Vis-NIR spectroscopy. All measurement were performed under N₂ atmosphere and were carried out in a sealed OTTLE (optically transparent thin-layer electrochemistry) cell using a platinum working electrode in dichloromethane (DCM) solutions with 0.25 M (nBu₄N)(PF₆) as supporting electrolyte. Electrolytic reduction was performed via stepwise 25 mV increments vs Ag/AgCl and the extant of the reduction and formation of MV states were monitored using Vis-NIR spectra. Spectra of electrolyzed solution of complex 1³⁺ display a decrease in the intensity of the isovalent parent absorbances at 624 and 618 nm and emergence of a new NIR transitions, ascribed to intervalence charge transfer (IVCT) transitions in the generated MV state (Figure S56). These transitions are subsequently suppressed as complex 1 is further reduced to the isovalent neutral oxidation state. Due to the low degree of separation of the $E^{0}_{1/2}$ of complex 1, sole in-situ formation of each MV state of complex 1 was not accessible, leading to mixtures of MV and isovalent likely observed in the Vis-NIR spectra. In contrast, spectra of electrolyzed solutions of complex 2^{3+} display the formation of three distinct species in solution, with clean isobestic points indicating facile conversion of each species to subsequent MV states (Figures 8 and S57). Facile formation of MV species of complex 2, such as 2²⁺ and 2⁺ (Figures 8a,c), is indicated by the emergence of absorbances in the near-IR, ascribed to intervalence charge transfer (IVCT) transitions in the generated MV state. Spectra of MV states 2²⁺ and 2⁺ were further deconvoluted and fit with gaussian peak forms and the characteristic peak energies (v_{max}), molar absorptivity (ε_{IVCT}), and peak width at half-heights ($\Delta v_{1/2}$) of the IVCT bands can be found in Table 5.

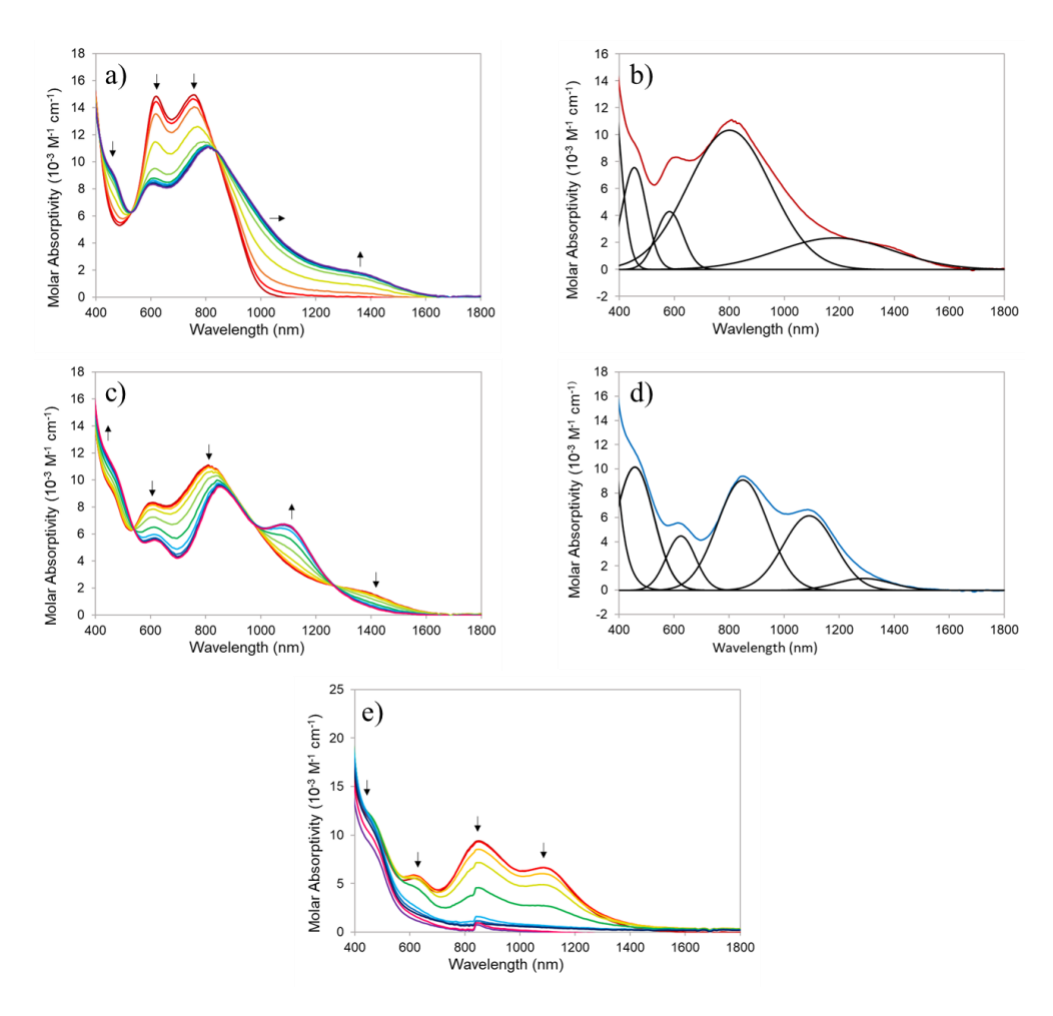


Figure 8. Vis-NIR spectra of the electrochemical reduction of 2^{3+} in a DCM solution of 0.25 M [nBu₄N][PF₆] under an atmosphere of N₂: a) 2^{3+} to 2^{2+} b) 2^{2+} c) 2^{2+} to 2^{4+} d) 2^{4+} e) 2^{4+} to 2^{0+} . Solution electrolyzed cathodically by 25 mV increments.

Table 5. IVCT characteristic values for complex **2** in the near-IR range.

Complex	Transition	v _{max} (cm ⁻¹) [nm]	$\begin{array}{c} \epsilon_{\rm IVCT} \\ (10^3~M^{\text{-}1}\\ \text{cm}^{\text{-}1}) \end{array}$	Δv _{1/2} (cm ⁻ 1)	Γ	$\begin{array}{c} \rm H_{ab} \\ (10^3 \\ \rm cm^{-1}) \end{array}$
2 ²⁺	V 1	8430	2.4	20440	-3.6	1.7
		[1186]				
2 ⁺	v ₂	9158	5.1	45040	-8.8	4.0
		[1092]				
	V 3	7749	0.81	42505	-9	1.4
		[1291]				

As 2^{3+} is electrochemically reduced to 2^{2+} , we observe a suppression of the isovalent parent transitions at 618 and 756 nm, and the emergence of two new absorption bands at 802 and 1186

nm (v₁), with the latter attributed to an IVCT (Figures 8a,b). As the potential is stepped further cathodically, the absorption bands in the visible region are further reduced in intensity, with two new NIR transitions developing at 1092 (v₂) and 1291nm (v₃), indicating the conversion of 2²⁺ to 2⁺ (Figures 8c,d). Lastly, as 2⁺ is reduced to the 2⁰, we observe a general decrease in intensity of absorption bands in both the visible and NIR spectrum, suggesting a conversion from the mixed-valent 2⁺ to the isovalent 2⁰ (Figures 8e). The degree of electronic coupling in complex 2 was further assessed using the electronic parameters of the IVCT bands obtained from spectra of 2²⁺ and 2⁺. The extent of electronic coupling in MV species has been classically distinguished between Class II (localized charge, weak to moderate coupling), borderline Class II-III (localized-delocalized charge, moderate coupling), and Class III (delocalized charge, strong coupling). ^{44–46} Using the classification method developed by Brunschwig, Creutz, and Sutin, the magnitude of divergence of the theoretical IVCT bandwidth from that of the experimental band width can inform on the degree of electronic coupling in the system (Equation 2): ⁴⁶

$$\Gamma = 1 - \left(\Delta v_{\frac{1}{2}} / \Delta v_{\frac{1}{2}}^{0}\right) \tag{2}$$

$$H_{ab} = \frac{2.06E^{-2} \left(v_{max} \varepsilon_{IVCT} \Delta v_{\frac{1}{2}} \right)^{1/2}}{r_{ab}}$$
 (3)

where $\Delta v^0_{1/2}$ is the theoretical IVCT bandwidth, which can be calculated according to the reported equation (see SI, Equation S2). The measured Γ values can be found in Table 4. Magnitude of the Γ values fall well below 0.1 indicating our system can be classified as a Class II localized system, in agreement with previous designation to the Co₃Cp*₃BHT. Based on this assignment, the proper equation can be employed to directly measure the electronic coupling parameter (Hab) for the detected IVCT transitions (Equation 3), where rab is the through-space geometrical distance between redox active sites in Å. 47,48 These values are located in Table 4. An intermetallic distance of 7.4 Å was chosen to be the distance between redox active sites (metal centers in this case) (r_{ab}) for the reported values for Co₃Cp*₃BHT and will be used in this study to allow for accurate comparison between both complexes. Additionally, this value is analogous to the cobalt-cobalt distance in the calculated geometrically optimized structure (7.467 Å, vide infra). It should be noted that the choice of rab is often a point of significant error in reported Hab values due to the inherent ambiguity in the effective charge transfer distance, and its congruity with formally assigned redox sites.⁴⁹ Utilizing the IVCT bands of complexes 2²⁺ and 2⁺ to measure H_{ab} values yields results that are an order of magnitude larger than those reported for Co₃Cp*₃BHT.² This difference in strength of electronic coupling in complex 2 compared to Co₃Cp*₃BHT is striking upon comparison with the previous similarities of comproportionation values for both these complexes. Spectroscopic analysis of the MV states can be more diagnostic of the true nature of electronic coupling in MV species, and as a result we conclude that complex 2 displays stronger electronic communication than Co₃Cp*₃BHT. As the free energy of comproportionantion is influenced by many different thermodynamic components such as inductive, magnetic exchange, and electrostatic contributions, other stabilizing/destabilizing components outside of electronic

coupling may be generating similar comproportionation values for complexes 2 and Co₃Cp*₃BHT.³⁵

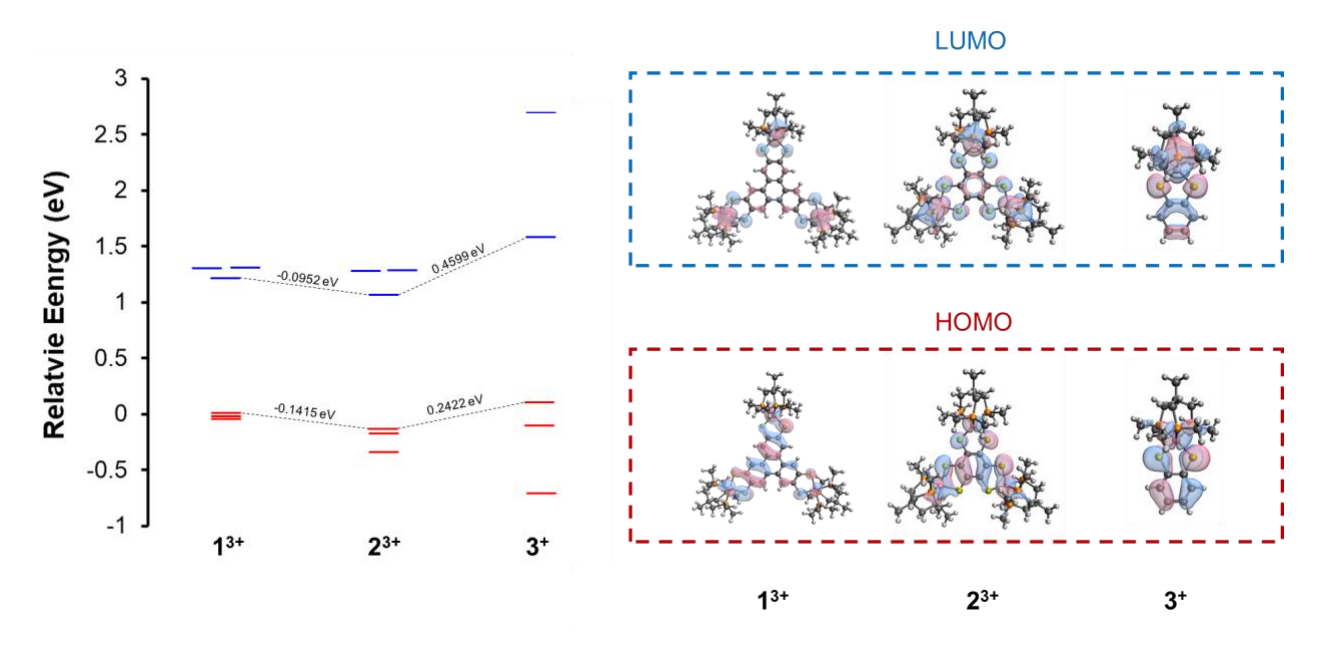


Figure 9. Molecular orbital scheme of complexes 1^{3+} , 2^{3+} , and 3^{+} (left), with the corresponding orbital character of HOMO and LUMO (right).

A series of unrestricted density functional theory (DFT) calculations at 6-31G*/PBE level of theory were performed on complexes 1^{3+} , 2^{3+} , and 3^{+} to supplement the experimental results (Figure 9). For calculations performed on complexes 1^{3+} , 2^{3+} , and 3^{+} , the aryl substituents of the triphos capping ligand were modeled as methyl groups to decrease computing complexity and time (Figures S43-S45). Based on these calculations, the highest occupied molecular orbitals (HOMOs) for all three complexes are primarily localized on the dithiolene ligand and exhibit $Co(d_{xy})$ - $S(p_z)$ π^* anti-bonding character (Figures 9, S47-S50). The lowest unoccupied molecular orbitals (LUMOs) of complexes 1^{3+} , 2^{3+} , and 3^+ yield orbitals that are metal-center dominant, with Co(d_z^2)- $P(p_z) \sigma^*$ and $Co(d_z^2)$ - $S(p_z) \pi^*$ antibonding character and considerable orbital contribution from the triphos ligand (Figures 9, S47-S49, and S51). Contribution of the dithiolene ligand to the LUMO follows a trend of $3^+ > 2^{3+} > 1^{3+}$ (Figures 9, S47-S49, and S51), suggesting stronger electronic exchange between metal sites in complex 2, compared to that in complex 1. This is also supported by the electrochemical studies discussed above. Compared to the frontier orbitals calculated for Co₃Cp^{*}₃THT, Co₃Cp^{*}₃BHT, and CoCp^{*}BDT, we do not observe a destabilization of the HOMOs of complexes 1³⁺ and 2³⁺ relative to that of complex 3⁺. Rather, an inverted relationship is observed in which the HOMO of complex 3^+ is destabilized relative to those of complexes 1^{3+} and 2^{3+} (destabilized by 0.1006 and 0.2422 eV compared to the HOMO of complex 1^{3+} and 2^{3+} , respectively, Figure 9 and Table S1). The LUMO of complex 3⁺ is also significantly destabilized compared to the LUMOs of complexes 13+ and 23+ (destabilized by 0.3646 and 0.4599 eV compared to the LUMOs of complex 1^{3+} and 2^{3+} , respectively). This difference may be due to the cationic nature of these complexes; the greater π -conjugation of complexes 1^{3+} and 2^{3+} leads to an overall stabilization of the charged system, in contrast to the neutral Co₃Cp*₃THT, Co₃Cp*₃BHT, and $CoCp^*BDT$ complexes.¹ Furthermore, comparison of the frontier orbitals of complexes 1^{3+} and 2^{3+} indicates a contrasting trend to that reported for $Co_3Cp^*_3THT$ and $Co_3Cp^*_3BHT$, where the frontier orbitals of complex 2^{3+} are slightly stabilized relative to those of complex 1^{3+} . This relationship can be rationalized as a stronger stabilization of the frontier orbitals of complex 2^{3+} due to the greater degree of conjugated coupling between metal centers through the benzene backbone of complex 2^{3+} compared to the weaker coupling through the larger triphenylene backbone in complex 1^{3+}_{-1} .

Time-dependent DFT (TD-DFT) calculations were carried out for complex 3 as a model system to establish a qualitative understanding for the observed electronic transitions of these complexes. The aryl substituents of the triphos ligand were explicitly included in these calculations to better clarify the role of the capping ligand in the observed transitions (Figure S46). Based on these calculations, the observed λ_1 transition for complex 3^+ at 540 nm can be principally attributed to a HOMO-LUMO transition, suggesting a singlet LMCT transition (Tables S2-S3, Figure S52). The weaker absorption band detected at 720 nm is calculated to involve contributions from HOMO-1, HOMO-7, and HOMO-12 to the LUMO in addition to a significant contribution from a HOMO-LUMO transition (Tables S2, S4-S5, Figures S53-S54). Due to significant involvement of the triphos capping ligand to these HOMO orbitals (Figures S53-S54), as well as contribution by the dithiolene ligand, a singlet LMCT transition is also consistent with this assignment. We attribute the transitions observed for complexes 1^{3+} and 2^{3+} to LMCT-type transitions based on these predictions, with the considerable broadening of the absorption bands resulting from the increased orbital degeneracies in these species (Figure 7). Significant contribution of the triphos ligand to the absorption at 720 nm for complex 3⁺ also suggests why these transitions are not present in the visible spectra of Co₃Cp*₃THT, Co₃Cp*₃BHT, and Co₃Cp*₃BDT. 11,20 Based on these calculations, we can determine the origin of the relative shifts displayed in the visible spectra of complexes 1^{3+} , 2^{3+} , and 3^{+} . As previously stated, a strong blue shift is observed in the absorption maxima for complex 3^+ , compared to complexes 1^{3+} and 2^{3+} . As the λ_1 transition at 624 nm is predicted to involve substantial contribution from a HOMO-LUMO transition, the shift in this peak can be rationalized by the destabilization of the LUMO of complex 3⁺ relative to that of complexes 1^{3+} and 2^{3+} . Similarly, the slight blue shift in the λ_1 transition of complex 2^{3+} compared to that of complex 1³⁺ can be rationalized as an increase in the HOMO-LUMO/(HOMO-1)-LUMO gap of complex 2^{3+} compared to that of complex 1^{3+} .

Conclusions

In summary, we report a series of trinuclear cobalt complexes incorporating triphenylene-2,3,6,7,10,11-hexathiolate (THT) (1³⁺), and benzene hexathiolate (BHT) (2³⁺) to provide insight into the electronic properties of the analogous cobalt-dithiolene 2-D MOFs. We have investigated the electronic coupling between multiple metal centers in the trimetallic systems as a function of the coordination sphere and the electrochemical medium, and have compared these results to those of the previously-reported Co₃Cp*₃THT and Co₃Cp*₃BHT complexes to clarify the role of the capping ligand.^{1,2} The solid state crystal structure of complex 1³⁺ reveals three five-coordinate cobalt centers that are bound to the triphos and the THT ligands in a distorted square pyramidal

geometry. Cyclic voltammetry (CV) studies of complexes 1 and 2 display three reversible redox events (assigned to the Co^{III/II} couple), resulting in the formation of mixed valence states following electronically-coupled sequential reductions of redox-active metal centers. comproportionality constants (Log K_c) based on the Co^{III/II} redox couples were determined to be 1.4 and 1.5 for complex 1, and 4.7 and 5.8 for complex 2. These results are similar to those reported for Co₃Cp*₃THT and Co₃Cp*₃BHT, suggesting minimal influence of the capping ligand on the stability of the MV states of complexes 1 and 2. Electrochemical studies in solvents of different polarities were conducted, which demonstrate that the $\Delta E_{1/2}$ of the Co^{III/II} couple shifts as a function of solvent polarity, indicating a negative correlation between polarity of the electrochemical medium and the stability of the species. UV-Vis absorption spectroscopy studies indicate a red shift in the absorption bands of complexes 1^{3+} and 2^{3+} compared to the monometallic congener 3^{+} . These transitions are not observed for Co₃Cp*₃THT and Co₃Cp*₃BHT, suggesting they are attributed to contributions from the triphos ligand. Spectroscopic analysis of electrochemically generated MV states of complexes 1 and 2 yield Vis-NIR spectra that display IVCT bands in the NIR. Analysis of the IVCT transitions for complex 2 indicate a class II localized MV species, with Hab values significantly larger than what is reported for Co₃Cp*₃BHT, suggesting stronger electronic communication in complex 2. Density functional theory (DFT) calculations predict a significant deviation in the relative energies of the frontier orbitals of complexes 1³⁺, 2³⁺, and 3⁺ that contrasts those calculated for Co₃Cp*₃THT and Co₃Cp*₃BHT, suggesting that the capping ligand contributes significantly to the overall electronic structure of the system.

ACKNOWLEDGMENT

The research was primarily supported by the U. S. Department of Energy, Office of Basic Energy Sciences, Division of Chemical Sciences, Geosciences and Biosciences under Award DE-SC0019236 (experimental studies), and the National Science Foundation under award DMR-2004868 (theoretical studies). XPS data was collected at the Core Center of Excellence in Nano Imaging, USC.

REFERENCES

- (1) Sakamoto, R.; Kambe, T.; Tsukada, S.; Takada, K.; Hoshiko, K.; Kitagawa, Y.; Okumura, M.; Nishihara, H. Π-Conjugated Trinuclear Group-9 Metalladithiolenes With a Triphenylene Backbone. *Inorg. Chem.* **2013**, *52* (13), 7411–7416. https://doi.org/10.1021/ic400110z.
- (2) Nishihara, H.; Okuno, M.; Akimoto, N.; Kogawa, N.; Aramaki, K. Synthesis of π-Conjugated Cobaltadithiolene Cyclotrimers and Significant Effects of Electrolyte Cation and Solvent on Their Electrochemical, Optical and Magnetic Properties. *J. Chem. Soc. Dalt. Trans.* **1998**, *I* (16), 2651–2656. https://doi.org/10.1039/a803028f.
- (3) Furukawa, H.; Cordova, K. E.; O'Keeffe, M.; Yaghi, O. M. The Chemistry and Applications of Metal-Organic Frameworks. *Science* (80-.). **2013**, 341 (6149), 1230444.

- https://doi.org/10.1126/science.1230444.
- (4) Zhou, H.-C.; Long, J. R.; Yaghi, O. M. Introduction to Metal–Organic Frameworks. *Chem. Rev.* **2012**, *112* (2), 673–674. https://doi.org/10.1021/cr300014x.
- (5) Sun, L.; Campbell, M. G.; Dincă, M. Electrically Conductive Porous Metal-Organic Frameworks. *Angew. Chemie Int. Ed.* **2016**, *55* (11), 3566–3579. https://doi.org/10.1002/anie.201506219.
- (6) Wang, M.; Dong, R.; Feng, X. Two-Dimensional Conjugated Metal—Organic Frameworks (2D c -MOFs): Chemistry and Function for MOFtronics. *Chem. Soc. Rev.* 2021. https://doi.org/10.1039/D0CS01160F.
- (7) Huang, X.; Sheng, P.; Tu, Z.; Zhang, F.; Wang, J.; Geng, H.; Zou, Y.; Di, C. A.; Yi, Y.; Sun, Y.; Xu, W.; Zhu, D. A Two-Dimensional π-d Conjugated Coordination Polymer with Extremely High Electrical Conductivity and Ambipolar Transport Behaviour. *Nat. Commun.* 2015, 6, 6–13. https://doi.org/10.1038/ncomms8408.
- (8) Sheberla, D.; Bachman, J. C.; Elias, J. S.; Sun, C. J.; Shao-Horn, Y.; Dincă, M. Conductive MOF Electrodes for Stable Supercapacitors with High Areal Capacitance. *Nat. Mater.* **2017**, *16* (2), 220–224. https://doi.org/10.1038/nmat4766.
- (9) Dong, R.; Zhang, Z.; Tranca, D. C.; Zhou, S.; Wang, M.; Adler, P.; Liao, Z.; Liu, F.; Sun, Y.; Shi, W.; Zhang, Z.; Zschech, E.; Mannsfeld, S. C. B.; Felser, C.; Feng, X. A Coronene-Based Semiconducting Two-Dimensional Metal-Organic Framework with Ferromagnetic Behavior. *Nat. Commun.* **2018**, *9* (1), 1–9. https://doi.org/10.1038/s41467-018-05141-4.
- (10) Downes, C. A.; Marinescu, S. C. Electrocatalytic Metal–Organic Frameworks for Energy Applications. *ChemSusChem* **2017**, *10* (22), 4374–4392. https://doi.org/10.1002/cssc.201701420.
- (11) Dong, R.; Zheng, Z.; Tranca, D. C.; Zhang, J.; Chandrasekhar, N.; Liu, S.; Zhuang, X.; Seifert, G.; Feng, X. Immobilizing Molecular Metal Dithiolene-Diamine Complexes on 2D Metal-Organic Frameworks for Electrocatalytic H 2 Production. *Chem. A Eur. J.* **2017**, *23* (10), 2255–2260. https://doi.org/10.1002/chem.201605337.
- (12) Kambe, T.; Sakamoto, R.; Kusamoto, T.; Pal, T.; Fukui, N.; Hoshiko, K.; Shimojima, T.; Wang, Z.; Hirahara, T.; Ishizaka, K.; Hasegawa, S.; Liu, F.; Nishihara, H. Redox Control and High Conductivity of Nickel Bis(Dithiolene) Complex π-Nanosheet: A Potential Organic Two-Dimensional Topological Insulator. *J. Am. Chem. Soc.* 2014, *136* (41), 14357–14360. https://doi.org/10.1021/ja507619d.
- (13) Banda, H.; Dou, J.-H.; Chen, T.; Libretto, N. J.; Chaudhary, M.; Bernard, G. M.; Miller, J. T.; Michaelis, V. K.; Dincă, M. High-Capacitance Pseudocapacitors from Li + Ion Intercalation in Nonporous, Electrically Conductive 2D Coordination Polymers. *J. Am. Chem. Soc.* **2021**, *143* (5), 2285–2292. https://doi.org/10.1021/jacs.0c10849.
- (14) Dong, R.; Han, P.; Arora, H.; Ballabio, M.; Karakus, M.; Zhang, Z.; Shekhar, C.; Adler, P.; Petkov, P. S.; Erbe, A.; Mannsfeld, S. C. B.; Felser, C.; Heine, T.; Bonn, M.; Feng, X.; Cánovas, E. High-Mobility Band-like Charge Transport in a Semiconducting Two-

- Dimensional Metal–Organic Framework. *Nat. Mater.* **2018**, *17* (11), 1027–1032. https://doi.org/10.1038/s41563-018-0189-z.
- (15) Huang, X.; Li, H.; Tu, Z.; Liu, L.; Wu, X.; Chen, J.; Liang, Y.; Zou, Y.; Yi, Y.; Sun, J.; Xu, W.; Zhu, D. Highly Conducting Neutral Coordination Polymer with Infinite Two-Dimensional Silver–Sulfur Networks. *J. Am. Chem. Soc.* **2018**, *140* (45), 15153–15156. https://doi.org/10.1021/jacs.8b07921.
- (16) Chen, I.-F.; Lu, C.-F.; Su, W.-F. Highly Conductive 2D Metal—Organic Framework Thin Film Fabricated by Liquid—Liquid Interfacial Reaction Using One-Pot-Synthesized Benzenehexathiol. *Langmuir* **2018**, *34* (51), 15754–15762. https://doi.org/10.1021/acs.langmuir.8b03938.
- (17) Clough, A. J.; Yoo, J. W.; Mecklenburg, M. H.; Marinescu, S. C. Two-Dimensional Metal-Organic Surfaces for Efficient Hydrogen Evolution from Water. *J. Am. Chem. Soc.* **2015**, *137* (1), 118–121. https://doi.org/10.1021/ja5116937.
- (18) Clough, A. J.; Skelton, J. M.; Downes, C. A.; De La Rosa, A. A.; Yoo, J. W.; Walsh, A.; Melot, B. C.; Marinescu, S. C. Metallic Conductivity in a Two-Dimensional Cobalt Dithiolene Metal-Organic Framework. *J. Am. Chem. Soc.* 2017, *139* (31), 10863–10867. https://doi.org/10.1021/jacs.7b05742.
- (19) Clough, A. J.; Orchanian, N. M.; Skelton, J. M.; Neer, A. J.; Howard, S. A.; Downes, C. A.; Piper, L. F. J.; Walsh, A.; Melot, B. C.; Marinescu, S. C. Room Temperature Metallic Conductivity in a Metal-Organic Framework Induced by Oxidation. *J. Am. Chem. Soc.* **2019**, *141* (41), 16323–16330. https://doi.org/10.1021/jacs.9b06898.
- (20) Chen, K.; Downes, C. A.; Goodpaster, J. D.; Marinescu, S. C. Hydrogen Evolving Activity of Dithiolene-Based Metal–Organic Frameworks with Mixed Cobalt and Iron Centers. *Inorg. Chem.* **2021**, *60* (16), 11923–11931. https://doi.org/10.1021/acs.inorgchem.1c00900.
- (21) Chen, K.; Downes, C. A.; Schneider, E.; Goodpaster, J. D.; Marinescu, S. C. Improving and Understanding the Hydrogen Evolving Activity of a Cobalt Dithiolene Metal-Organic Framework. *ACS Appl. Mater. Interfaces* **2021**, *13* (14), 16384–16395. https://doi.org/10.1021/acsami.1c01727.
- (22) Dong, R.; Pfeffermann, M.; Liang, H.; Zheng, Z.; Zhu, X.; Zhang, J.; Feng, X. Large-Area, Free-Standing, Two-Dimensional Supramolecular Polymer Single-Layer Sheets for Highly Efficient Electrocatalytic Hydrogen Evolution. *Angew. Chemie Int. Ed.* **2015**, *54* (41), 12058–12063. https://doi.org/10.1002/anie.201506048.
- (23) Huang, X.; Zhang, S.; Liu, L.; Yu, L.; Chen, G.; Xu, W.; Zhu, D. Superconductivity in a Copper(II)-Based Coordination Polymer with Perfect Kagome Structure. *Angew. Chemie Int. Ed.* **2018**, *57* (1), 146–150. https://doi.org/10.1002/anie.201707568.
- (24) Cui, J.; Xu, Z. An Electroactive Porous Network from Covalent Metal–Dithiolene Links. *Chem. Commun.* **2014**, *50* (30), 3986–3988. https://doi.org/10.1039/C4CC00408F.
- (25) Grange, C. S.; Meijer, A. J. H. M.; Ward, M. D. Trinuclear Ruthenium Dioxolene Complexes Based on the Bridging Ligand Hexahydroxytriphenylene: Electrochemistry,

- Spectroscopy, and near-Infrared Electrochromic Behaviour Associated with a Reversible Seven-Membered Redox Chain. *Dalt. Trans.* **2010**, *39* (1), 200–211. https://doi.org/10.1039/b918086a.
- (26) Yang, L.; He, X.; Dincă, M. Triphenylene-Bridged Trinuclear Complexes of Cu: Models for Spin Interactions in Two-Dimensional Electrically Conductive Metal-Organic Frameworks. *J. Am. Chem. Soc.* **2019**, *141* (26), 10475–10480. https://doi.org/10.1021/jacs.9b04822.
- (27) Yang, L.; Dincă, M. Redox Ladder of Ni3 Complexes with Closed-Shell, Mono-, and Diradical Triphenylene Units: Molecular Models for Conductive 2D MOFs. *Angew. Chemie Int. Ed.* **2021**, *60* (44), 23784–23789. https://doi.org/10.1002/anie.202109304.
- (28) Downes, C. A.; Clough, A. J.; Chen, K.; Yoo, J. W.; Marinescu, S. C. Evaluation of the H2 Evolving Activity of Benzenehexathiolate Coordination Frameworks and the Effect of Film Thickness on H2 Production. *ACS Appl. Mater. Interfaces* **2018**, *10* (2), 1719–1727. https://doi.org/10.1021/acsami.7b15969.
- (29) Asam, A.; Janssen, B.; Huttner, G.; Zsolnai, L.; Walter, O. Tripod-Eisen- Und Tripod-Cobalt-Komplexe Mit Acetonitril Als Stützliganden (Tripod = RCH2C(CH2PPh2)3; R = H, Ph) / Tripod-Iron and Tripod-Cobalt-Complexes with Acetonitrile as Supporting Ligands (Tripod = RCH2C(CH2PPh2)3; R = H, Ph). *Zeitschrift für Naturforsch. B* **1993**, 48 (12), 1707–1714. https://doi.org/10.1515/znb-1993-1202.
- (30) Ghilardi, C. A.; Laschi, F.; Midollini, S.; Orlandini, A.; Scapacci, G.; Zanello, P. Synthesis, Crystal Structure, Electrochemistry and Electronic Paramagnetic Resonance Spectroscopy of [M{(PPh2CH2)3CMe}(o-S2C6H4)][PF6] n (M = Fe, Co or Rh; N= 0 or 1). *J. Chem. Soc. Dalt. Trans.* **1995**, *1* (4), 531. https://doi.org/10.1039/dt9950000531.
- (31) Vogel, S.; Huttner, G.; Zsolnai, L. Fünffach Koordinierte Co(III)-Komplexe [Tripod-Cobalt-(Ortho(X)(Y)C6H4)] + Mit Ortho-Phenylenverbrückten Chelatliganden [(XH)(YH)C 6 H 4] (XH, YH = NH2, OH, SH). *Zeitschrift für Naturforsch. B* **1993**, *48* (5), 641–652. https://doi.org/10.1515/znb-1993-0514.
- (32) Beswick, C. L.; Schulman, J. M.; Stiefel, E. I. Structures and Structural Trends in Homoleptic Dithiolene Complexes. In *Progress in Inorganic Chemistry, Vol. 52*; Karlin, K. D., Ed.; Wiley-Interscience: Hoboken, 2004; pp 55–110. https://doi.org/10.1002/0471471933.ch2.
- (33) Shibata, Y.; Zhu, B.; Kume, S.; Nishihara, H. Development of a Versatile Synthesis Method for Trinuclear Co(Iii), Rh(Iii), and Ir(Iii) Dithiolene Complexes, and Their Crystal Structures and Multi-Step Redox Properties. *J. Chem. Soc. Dalt. Trans.* **2009**, No. 11, 1939–1943. https://doi.org/10.1039/b815560g.
- (34) Creutz, C. Mixed Valence Complexes of d 5 d 6 Metal Centers. In *Progress in Inorganic Chemistry: An Appreciation of Henry Taube*; Lippard, S. J., Ed.; Wiley interscience: new york, 2007; Vol. 30, pp 1–73. https://doi.org/10.1002/9780470166314.ch1.
- (35) Richardson, D. E.; Taube, H. Mixed-Valence Molecules: Electronic Delocalization and Stabilization. *Coord. Chem. Rev.* **1984**, *60*, 107–129. https://doi.org/10.1016/0010-8545(84)85063-8.

- (36) Evans, C. E. B.; Naklicki, M. L.; Rezvani, A. R.; White, C. A.; Kondratiev, V. V.; Crutchley, R. J. An Investigation of Superexchange in Dinuclear Mixed-Valence Ruthenium Complexes. *J. Am. Chem. Soc.* **1998**, *120* (50), 13096–13103. https://doi.org/10.1021/ja982673b.
- (37) Crutchley, R. J. Intervalence Charge Transfer and Electron Exchange Studies of Dinuclear Ruthenium Complexes. *Adv. Inorg. Chem.* **1994**, *41*, 273–325. https://doi.org/10.1016/S0898-8838(08)60174-9.
- (38) Wohlfarth, C. W. Permittivity (Dielectric Constant) of Liquids. In *CRC Handbook of Chemistry and Physics*; Rumble, J., Ed.; CRC Press, 2021; pp 6-187-6–208.
- (39) Barrière, F.; Geiger, W. E. Use of Weakly Coordinating Anions to Develop an Integrated Approach to the Tuning of ΔΕ1/2 Values by Medium Effects. *J. Am. Chem. Soc.* **2006**, *128* (12), 3980–3989. https://doi.org/10.1021/ja058171x.
- (40) Nelsen, S. F.; Weaver, M. N.; Telo, J. P. Solvent Control of Charge Localization in 11-Bond Bridged Dinitroaromatic Radical Anions. *J. Am. Chem. Soc.* **2007**, *129* (22), 7036–7043. https://doi.org/10.1021/ja067088m.
- (41) Sutton, J. E.; Sutton, P. M.; Taube, H. Determination of the Comproportionation Constant for a Weakly Coupled Mixed-Valence System by Titration of the Intervalence Transfer Band: μ-(4, 4'-Bipyridyl)-Bis(Pentaammineruthenium)(5+). *Inorg. Chem.* **1979**, *18* (4), 1017–1021. https://doi.org/10.1021/ic50194a028.
- (42) Inkpen, M. S.; Long, N. J.; Albrecht, T. Branched Complexes for Molecular Electronics, 2013.
- (43) Gutmann, V. Solvent Effects on the Reactivities of Organometallic Compounds. *Coord. Chem. Rev.* **1976**, *18* (2), 225–255. https://doi.org/10.1016/S0010-8545(00)82045-7.
- (44) Robin, M. B.; Day, P. Mixed Valence Chemistry-A Survey and Classification. In *Advances in Inorganic Chemistry and Radiochemistry*; 1968; Vol. 10, pp 247–422. https://doi.org/10.1016/S0065-2792(08)60179-X.
- (45) Nelsen, S. F. "Almost Delocalized" Intervalence Compounds. *Chem. A Eur. J.* **2000**, *6* (4), 581–588. https://doi.org/10.1002/(sici)1521-3765(20000218)6:4<581::aid-chem581>3.0.co;2-e.
- (46) Brunschwig, B. S.; Creutz, C.; Sutin, N. Optical Transitions of Symmetrical Mixed-Valence Systems in the Class II-III Transition Regime. *Chem. Soc. Rev.* **2002**, *31* (3), 168–184. https://doi.org/10.1039/b008034i.
- (47) Hush, N. S. Theoretical Considerations and Spectroscopic Data. *Prog. Inorg. Chem.* **1967**, 8, 391–444.
- (48) Hush, N. S. Homogeneous and Heterogeneous Optical and Thermal Electron Transfer. *Electrochim. Acta* **1968**, *13* (5), 1005–1023. https://doi.org/10.1016/0013-4686(68)80032-5.
- (49) Demadis, K. D.; Hartshorn, C. M.; Meyer, T. J. The Localized-to-Delocalized Transition in Mixed-Valence Chemistry. **2001**, *2* (Cl).

Table of contents graphic:

